Numerical Prediction for Temperature Profile of Parts Manufactured using Fused Filament Fabrication

H.R. Vanaei [a,b,*], S. Khelladi [a], M. Deligant [a], M. Shirinbayan [b], A. Tcharkhtchi [b]

[a] Arts et Metiers Institute of Technology, CNAM, LIFSE, HESAM University, Paris, France
[b] Arts et Metiers Institute of Technology, CNRS, CNAM, PIMM, HESAM University, Paris, France

A B S T R A C T

Bonding of parts produced by fused filament fabrication (FFF) significantly depends on the temperature profile of filaments depositing one top of each other. It is necessary to evaluate the temperature profile during fabrication of structures using both theoretical and experimental approaches. This work describes the overall heat transfer (using finite volume method) that exists in such a process by taking into account the possible phenomena that are developing during the manufacturing sequence: conduction between filaments, conduction between filament and support, and convection with the environment. Although the developed model is general and applicable to both amorphous and semi-crystalline polymers and/or composites, the recordings of temperature variation at the interface of adjacent filaments of a printed vertical wall of PLA illustrated good agreement by implementing very small K-type thermocouples in parallel. It is particularly concerning the occurrence of re-heating peaks during the deposition of new filaments onto previously deposited ones. The sensitivity of the developed code to the operating conditions is shown by variation of several parameters. This makes it easy to apply it for optimization purposes. Theoretical modeling and experimental data presented in this study help better understanding of heat transfer existing in polymer/composite additive manufacturing, and can be valuable to predict more accurately the bond quality and apply the obtained findings for further steps.

1. Introduction

The problem of effective bonding, reduced strength, and mechanical performance of fused filament fabrication (FFF)-printed 3D models [1–3] is still a major concern in 3D-printed structures [4,5]. Fused filament fabrication (FFF) – also known as 3D printing [6,7] – is an extensive classification of additive manufacturing (AM) processes [8] producing prototypes in various applications, such as aerospace, medical, automotive, etc. [9–15].

Several process parameters (including liquefier and platform temperature [16–21], print speed [22–24], infill percentage and pattern [25–27], and layer thickness [18,24,28]) affect the quality of the built part. Meanwhile, numerous heat transfer processes take place during FFF that have emotional impact on the part quality [29–32]. The stated parameters effectively play a critical role in the temperature evolution of deposited layers. Believably, this temperature gradient through the deposited layers stands bonding between filaments [33–37]. During the material deposition process, a hot layer that is extruded to the previously deposited layer, generates a small gap of time where the polymer-polymer interface is in a specific zone of temperature. It is above glass transition temperature (T_g: in amorphous materials such as acrylonitrile butadiene styrene [ABS]) or crystallization temperature (T_c: in semi-crystalline materials such as polylactic acid [PLA]) and below melting temperature, T_m ($T_g < T < T_m$ or $T_c < T < T_m$) [38–40]. Despite the diversity of works on mechanical strength of 3D-printed parts [26,41], several works addressed the evolution of temperature profile as a key parameter altering the bonding quality [42]. In general, each filament should be sufficiently hot during deposition, but not too hot, to avert deformation due to gravity and to the weight of the filaments deposited in subsequent layers; on the contrary, it should remain hot enough to certify adequate bonding with the adjacent filaments [43].

In the literature, numerous works addressed thermal modeling and measurements of temperature evolution in FFF [29,44,45]. Finite element simulations have been carried out to model cooling stages of FFF during deposition at various inputs [46]. 2D transient heat transfer analysis has been developed. It aimed at solidification investigation of a filament in a vertical stack representing a lower cooling rate that inspires the bonding [47]. Heat transfer through successive layers has also

Corresponding author at: Arts et Metiers Institute of Technology, CNAM, LIFSE, HESAM University, Paris, France.
E-mail address: hamidreza.vanaei@ensam.eu (H.R. Vanaei).

been numerically simulated showing the effect of print speed on bonding between adjacent filaments [42]. A computational approach has been proposed to predict bonding quality of adjacent filaments [43]. Significant numerical researches have also been carried out on understanding the heat conducted from the liquefier and platform while the polymer is embedded through the liquefier and consequently deposited on the platform [29–31,45].

Alongside the significant numerical researches, experimental monitoring of temperature has exclusively revealed stimulating in FFF. Thermocouples have been employed to execute local measurement; however, the deposition might be interrupted while fixing a thermocouple [48]. A recent attempt was found by employing K-type thermocouples (d = 80 μm) in parallel to the deposition without pausing the route, which allows having a local measurement of temperature at the interface of adjacent filaments [49]. Furthermore, infrared (IR) thermography has been used in surface temperature measurement of filaments as an alternative approach due to the non-contact nature of recording [50–52]. The application of IR-camera in determination of the temperature profile of a vertical wall has demonstrated a good agreement with the applied theoretical prediction [53].

The state-of-the-art indicates that FFF is still in its early stage and there is still a noticeable gap in physical aspects such as thermal and rheological behavior. The temperature evolution during FFF thoroughly specified the quality and mechanical strength of fabricated structures [42]. Analytical investigation and experimental monitoring are still challenging in FFF and lack of practical knowledge corresponds to the problem of bonding in this process. Since the rheological properties are a function of temperature, together with mentioned process parameters, are widely affected by temperature evolution of filament while printing. To sum up, investigation on the temperature evolution of FFF is a missing spot, and itself governs the bonding quality.

This work is a first step toward the optimization of FFF process and quality improvement of 3D-printed parts. In fact, the developed approach is a global code considering complex geometries, physical phenomena (e.g. solidification, re-melting, rheological behavior), and it is applicable to different types of polymeric/composite materials. Here, we present the heat transfer using finite volume method (FVM) to execute the temperature evolution of deposited filaments in FFF. Besides, the developed temperature measurement technique allows to implement the experimental data for validation purposes [54]. The originality of this work includes the fact that the authors have focused on heat transfer mechanisms using an original mesh strategy by combining the Lagrangian and Eulerian methods. The simulation demonstrates the nozzle deposition by adding cells at the nozzle head-tip. Meanwhile, the heat transfer and temperature evolution are computed for the existing mesh considering dynamic mesh combined approach. Regarding the diffusion equation, the governing equation is approximated in terms of cell-centered scheme. An explicit scheme of the final equation is identified relying upon the discretization method by writing the mathematical physics equation. In FV form, the validated theoretical model is also applied in some case studies by the means of both predictive approach and experimental validation. Heat transfer code and measurements obtained in this study will help optimizing the FFF for adequate bonding quality.

Presumably, the paper is organized as follows: Sections 2 and 3 explain the mathematical modeling. Section 4 presents the experiment and measurement equipment. Section 5 discusses the analytical and experimental results as well as the usefulness of the developed code in some case studies. Finally, we conclude on the overall work.

2. Conservation equation

The conservation equation governing the heat transfer in (FFF)-3D printing is given by:

$$\frac{\partial}{\partial t}(\rho T) + div(\rho u T) = div(\Gamma grad T) + S_T \tag{1}$$

where Γ is diffusion coefficient and S is the source term. Finite volume method (FVM) [55] is a good candidate to solve numerically Eq. 1. In this work, a FVM heat transfer code is applied in order to perform the temperature evolution of deposited filaments in FFF process.

3. Numerical method

3.1. Finite volume method

In our case, FVM consists of performing a heat transfer balance over a given infinitesimal volume. Based on the experience of Khelladi et al. [56–58] in application of this method to several scientific problems, volume integrals of a partial differential equation are converted to the full surface. So, in the finite volume approach, the governing equations under their conservative form are widely used and the aim is to ensure that all characteristics remain similar in each cell/volume control. The main features of FVM could be mentioned as follows:

- Subdivision of the problem extent into non-overlapping control volumes (CVs)
- Consolidation of the governing equations (in our case: heat equation) over the CVs
- Evaluation of the integrals using the temperature variation between the grid points
- Representation of the conservation principle for the finite control volume using the obtained discretized equation

3.2. Problem formulation

We consider solving a two-dimensional unsteady heat conduction problem on a vertical wall of rectangular shape with the dimension of 50 * 0.4 * 35 mm. This test case was designed to predict the heat transfer during deposition of filaments based on the following assumptions:

- Same physical contact between filament and filament/support: the unidirectional deposition of filaments on top of each other gives the possibility of assuming same contact between the deposited layers
- Constant heat transfer coefficient between filament and air: this point is based on the same physical contact and it helps having more homogeneous temperature gradient
- Same printing strategy for all layers: this is necessary due to the temperature gradient and the cooling mechanism in deposited layers
- More homogeneity in temperature distribution: this relates to the fact that the mechanism of cooling and re-heating of filaments at every point and layer remains similar

Maintaining the first term of Eq. 1 in the discretization process, the finite volume integration of Eq. 1 over the CV by replacing the convective and diffusive terms with surface integrals obtained as follows:

$$\int_{CV} \frac{\partial(\rho T)}{\partial t} dV + \int_{CV} div(\rho T u) dV = \int_{CV} div(\Gamma grad T) dV + \int_{CV} S_T dV \tag{2}$$

By using Gauss divergence theorem, we obtain:

$$\int_{\Delta t} \frac{\partial}{\partial t} \left(\int_{CV} (\rho T) dV \right) dt + \int_{\Delta t} \int_{A} n(\rho T u) dA dt = \int_{\Delta t} \int_{A} n(\Gamma_T grad T) dA dt + \int_{\Delta t} \int_{CV} S_T dV dt \tag{3}$$

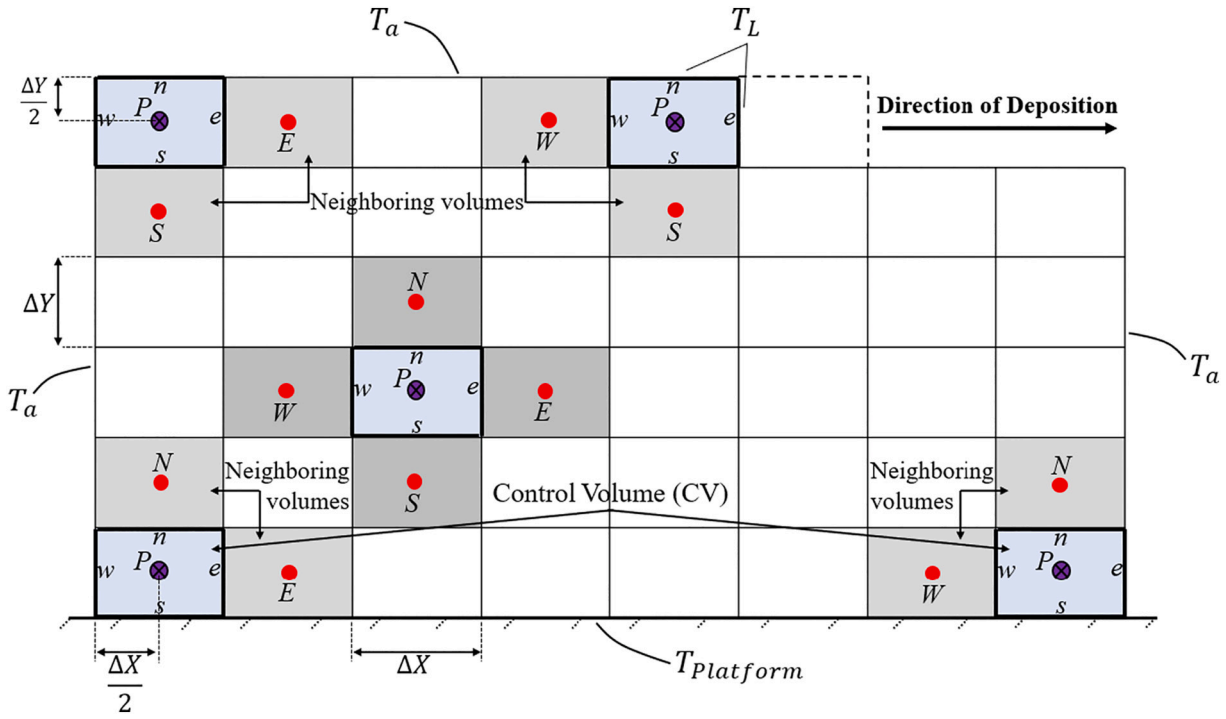

Fig. 1. Schematic of the object in finite volumes (T_{Liq}: liquefier temperature, $T_{Platform}$: platform temperature, T_a: ambient temperature, N: North, S: South, W: West, E: East).

3.3. Grid generation

The first step in launching FVM refers to the generation of grids by dividing the applicable area into the small discrete CVs to be considered as a C++ code. The borders of CVs are positioned halfway in between the adjacent nodes which itself is surrounded by control volume/cell. Fig. 1 indicates a rectangular domain divided into non-overlapping CVs. They are divided by dashed-lines introducing the boundaries of the individual CVs. These patterns that are created by the mentioned dashed-lines are called the computational grids. A general nodal point 'P' is specified by its neighbors, in a 2D geometry, nodes on north, south, west, and east; N, S, W, and E, respectively. As shown in Fig. 1, two sets of grid lines could be defined as follows: the grid lines defining the location of nodes, and those defining the CV faces.

So, the nodal point P is always placed in the geometric center of its CV with the following destinations:

$$y_P - y_s = y_n - y_P = \frac{\Delta y}{2}$$

$$x_P - x_w = x_e - x_P = \frac{\Delta x}{2}$$

Notably, lower case subscripts refer to the locations of the CV faces; whereas the upper case subscripts refer to the locations of the nodes. So, it is important to distinguish between upper and lower letters.

3.4. Discretization

Integration of governing equation on a CV is the most important characteristic of the FVM. The idea is to obtain a discretized equation to its nodal point P. The unsteady two-dimensional diffusion equation is as follows:

$$\rho C\frac{\partial T}{\partial t} = \frac{\partial}{\partial X}\left(K\frac{\partial T}{\partial X}\right) + \frac{\partial}{\partial Y}\left(K\frac{\partial T}{\partial Y}\right) + S \tag{4}$$

By integrating Eq. 4 over the CV and a time interval from t to $t + \Delta t$, we have:

$$\int_t^{t+\Delta t}\int_{CV}\rho C\frac{\partial T}{\partial t}\,dVdt = \int_t^{t+\Delta t}\int_{CV}\frac{\partial}{\partial X}\left(K\frac{\partial T}{\partial X}\right)dVdt + \int_t^{t+\Delta t}\int_{CV}\frac{\partial}{\partial Y}\left(K\frac{\partial T}{\partial Y}\right)dVdt + \int_t^{t+\Delta t}\int_{CV} SdVdt \tag{5}$$

This may be written as:

$$\int_t^{t+\Delta t}\int_{CV}\rho C\frac{\partial T}{\partial t}\,dVdt = \int_t^{t+\Delta t}\int_{CV}\left[\left(KA\frac{\partial T}{\partial X}\right)_e - \left(KA\frac{\partial T}{\partial X}\right)_w\right] + \int_t^{t+\Delta t}\int_{CV}\left[\left(KA\frac{\partial T}{\partial Y}\right)_n - \left(KA\frac{\partial T}{\partial Y}\right)_s\right] + \int_t^{t+\Delta t}\bar{S}dVdt \tag{6}$$

where A is the face area of the control volume, ΔV is its volume ($\Delta V = A\Delta X = A\Delta Y$), and $\bar{S}$ is the average source strength. Considering the following statements: (1) temperature at node P is implemented to the CV, (2) temperature at time t is assumed as ${T_P}^0$, (3) substituting $(T_p - {T_P}^0)/\Delta t$ for $\frac{\partial T}{\partial t}$, and (4) assuming the two-dimensional CV for discretization, the resulting equation over the two-dimensional CV is as follows:

$$a_P T_P = a_W T_W + a_E T_E + a_S T_S + a_N T_N + a_P^0 T_P^0 + S_u \tag{7}$$

where

$$a_P = a_W + a_E + a_S + a_N + a_P^0 - S_P$$

$$a_P^0 = \rho c\frac{\Delta V}{\Delta t}$$

The neighboring coefficients are given as follows:

$$a_N = \frac{\Gamma_n A_n}{\delta y_{PN}}$$

Table 1
Constant material properties of PLA (adapted from manufacturer) and boundary conditions used during FFF simulation.

Parameters	Value
Liquefier temperature (°C)	210
Platform temperature (°C)	50
Print speed (mm/s)	20
layer height (mm)	0.2
Test case dimension (mm)	50 * 0.4 * 35
Filament cross-section	Circular
Specific heat capacity (J/kg·K)	2100
Conductivity (W/m·K)	0.201
Melt flow index	6 g/10 min
Density (kg/m^3)	1250

$$a_S = \frac{\Gamma_s A_s}{\delta y_{SP}}$$

$$a_W = \frac{\Gamma_w A_w}{\delta x_{WP}}$$

$$a_E = \frac{\Gamma_e A_e}{\delta x_{PE}}$$

3.5. Boundary conditions

Alongside with the parameters related to the implemented material, the boundary conditions are defined as follows:

- North boundary: fixed temperature equal to the liquefier temperature
  - Cell in front of the liquefier: fixed temperature equal to the liquefier temperature
  - Other cells: fixed temperature equal to the ambient temperature
- South boundary: fixed temperature equal to the support temperature
- West boundary: fixed temperature equal to the ambient temperature
- East boundary: fixed temperature equal to the ambient temperature
- Front and back boundary: thermal source

As the code is in 2D, particular attention has been taken into account in definition of the boundary conditions. Accordingly, a thermal source has been added through the front and back boundaries to be implemented to the conservation equation that lets us considering the convection with the environment. This makes it possible to have a 3D implicit scheme for our modeling. Worth mentioning to say that the rapid calculation of the temperature profile in a small period of time ($1<t<2$ min), even with very small mesh, gives the possibility of performing simultaneous calculations in several points. Using the open-source software for compiling C++ codes, the calculations were obtained for extracting the temperature profile of filaments in the shortest possible time.

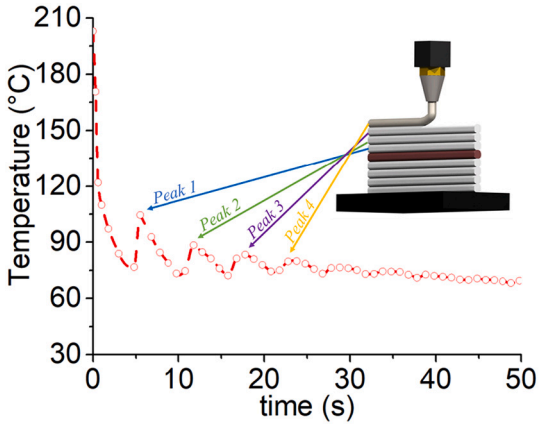

Fig. 3. Temperature evolution of layer 5 (at x = 30 mm) during the deposition of the vertical wall consisting of single filaments deposited on top of each other: Peaks 1, 2, 3, and 4 are re-heating of 5th filament (layer 5) by deposition of 6th, 7th, 8th, and 9th, respectively.

4. Experimental validation

4.1. Materials

To implement the experimental procedure and method validation, a commercially polylactic acid (PLA) filament with the diameter of d = 1.75 ± 0.01 mm has been used. As a semi-crystalline material, PLA has a crystallization temperature T_c = 102 °C with a melting point of T_m = 150 °C [49]. To perform the experiment, the test case was built using the value for the processing variables as indicated in Table 1. These values

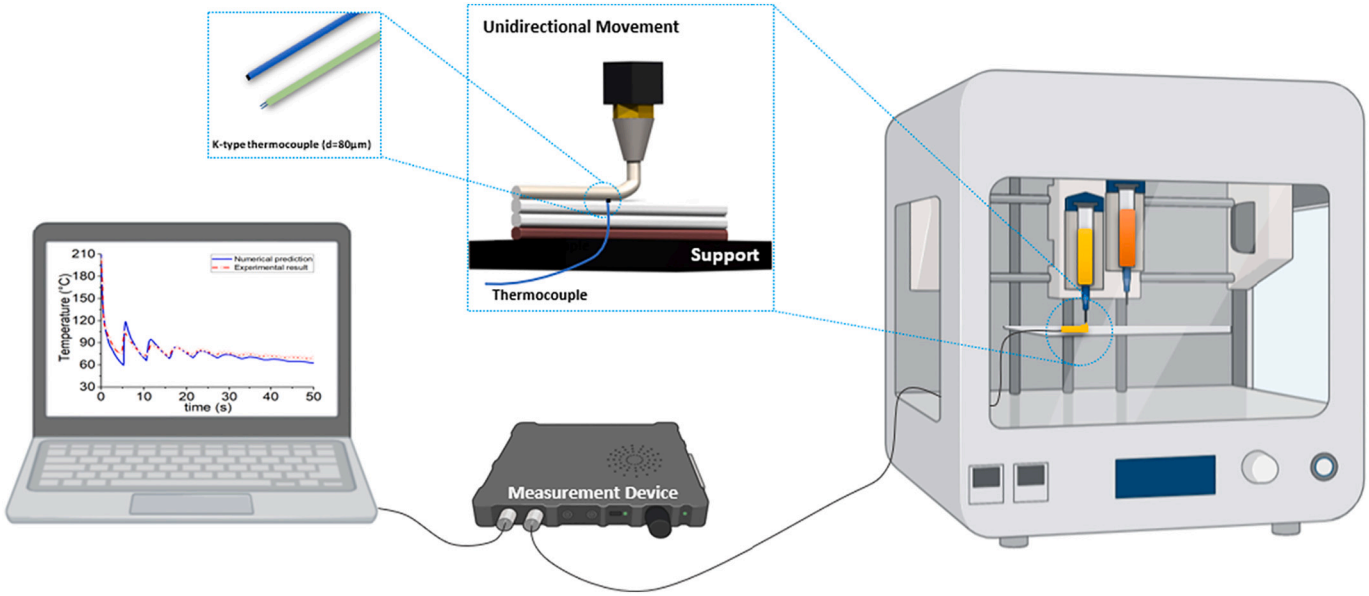

Fig. 2. Set-up of in-process monitoring of temperature profile during the deposition stage in FFF process.

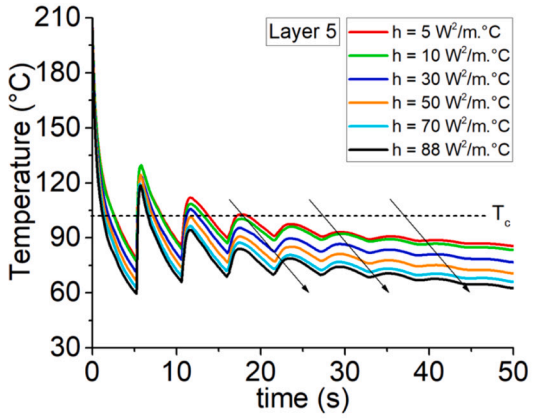

(a)

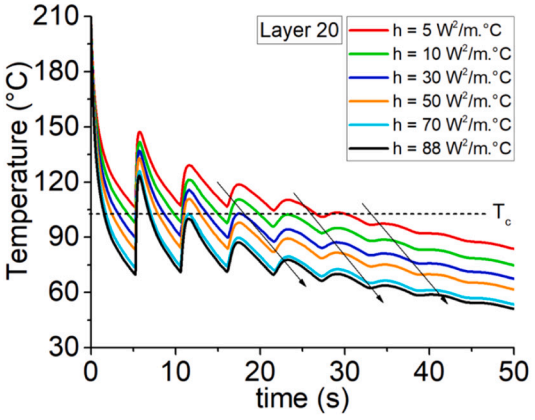

(b)

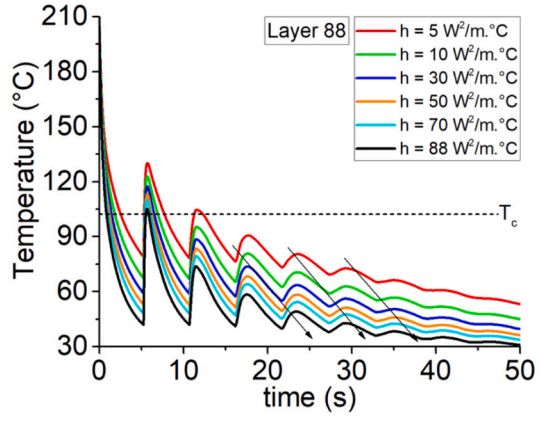

(c)

Fig. 4. The effect of h_{conv} on filament cooling: temperature evolution for h_{conv} = 5, 10, 30, 50, 70, and 88 W/m^2.°C of (a) Layer 5, (b) Layer 20, and (c) Layer 88.

have been chosen according to the literature [17,38,49]. At this stage, the objective is to ensure an acceptable quality part in terms of bonding and adhesion of different layers.

4.2. Measurement equipment

To track filament cooling and the re-heating peaks of deposition of successive layers, very small (d = 80 μm) K-type thermocouples were used (see [54] for method description). Set-up of the experiment is presented schematically in Fig. 2 containing the set-up for in-process measurement of temperature profile during the deposition stage.

5. Results and discussion

5.1. Local temperature profile

The graph presented in Fig. 3 provides the experimental results of the recorded temperature profile by implementing K-type thermocouples at the interface of adjacent filaments. As mentioned, the recorded experiment is based on layer-by-layer filament deposition. Under the defined 3D printing condition (the same for those using in parametric study), the previously deposited filament(s) has sufficiently cooled down. As an example (according to Fig. 3), the first cooling curve corresponds to the cooling of layer 5 (at the specific location) by deposition of younger filaments, a cyclic cooling and re-heating evolution appears to this layer which could be described as follows:

- 1st re-heating: re-heating of layer 5 by deposition of layer 6.
- 2nd cooling: cooling of layer 5 after deposition of layer 6.
- 2nd re-heating: re-heating of layer 5 by deposition of layer 7.
- 3rd cooling: cooling of layer 5 after deposition of layer 7.
- 3rd re-heating: re-heating of layer 5 by deposition of layer 8.
- Peaks 1, 2, 3, 4, etc.: re-heating peaks at the instant of deposition of layers 6, 7, 8, and 9, respectively.

Alongside with the above descriptions, one can note the influence of this cyclic temperature profile on adhesion and bonding of subsequent layers. In this case, it is obvious that after almost 4 to 5 filament deposition, the influence of deposition sequence is negligible. By using PLA (as a semi-crystalline material with crystallization temperature T_c = 102 °C [49]), the variation of temperature around T_c is inevitable and plays an important role in the adhesion of layers [59]. This is a key point to the importance of re-heating peaks in which they are progressively incapable of raising the temperature of previously deposited layers [49,52]. As a note, the latent heat of the PLA is not included in the code as it is going to be the next part of the proposed approach: adhesion of the layers.

5.2. Convection with the environment

Convective heat transfer that exists in FFF process has almost been investigated in literature [60]. According to the developed numerical code and to evaluate its functionality, the temperature evolution during 50 s of cooling of the vertical wall deposition at different locations has been presented. For post-processing, all signals are synchronized at $t = 0$ s based on the instant of the first recorded temperature (the highest measured value considered as a value at t = 0 s). The obtained results regarding the heat exchanges by convection for h = 5, 10, 30, 50, 70, and 88 W/m^2.°C have shown that the effect of this coefficient is evident, particularly on the cooling rate and temperature peaks. This could be clearly seen in Fig. 4 for random locations (as highlighted for layers 5, 20, and 88). A value of h_{conv} = 70 W/m^2.°C is normally used [61] and as it increased from 5 to 70 W/m^2.°C, the cooling rate increased and its effect is remarkable on the re-heating peaks. Besides, using the Churchill correlation for cooling of a cylinder by natural convection, h_{conv} = 88 W/m^2.°C was obtained which has been taken into account for the computation [54,62].

Fig. 5 shows the temperature evolution of filaments at specific instants upon constructing the vertical wall. Following the results reported above, under these printing conditions, deposition of a new filament causes the re-heating of those that have already been cooled down. Presenting a general overview in Fig. 5(a), the temperature evolution over the CVs has been recorded for layers 5, 10, and 43, respectively (Fig. 5(b)).

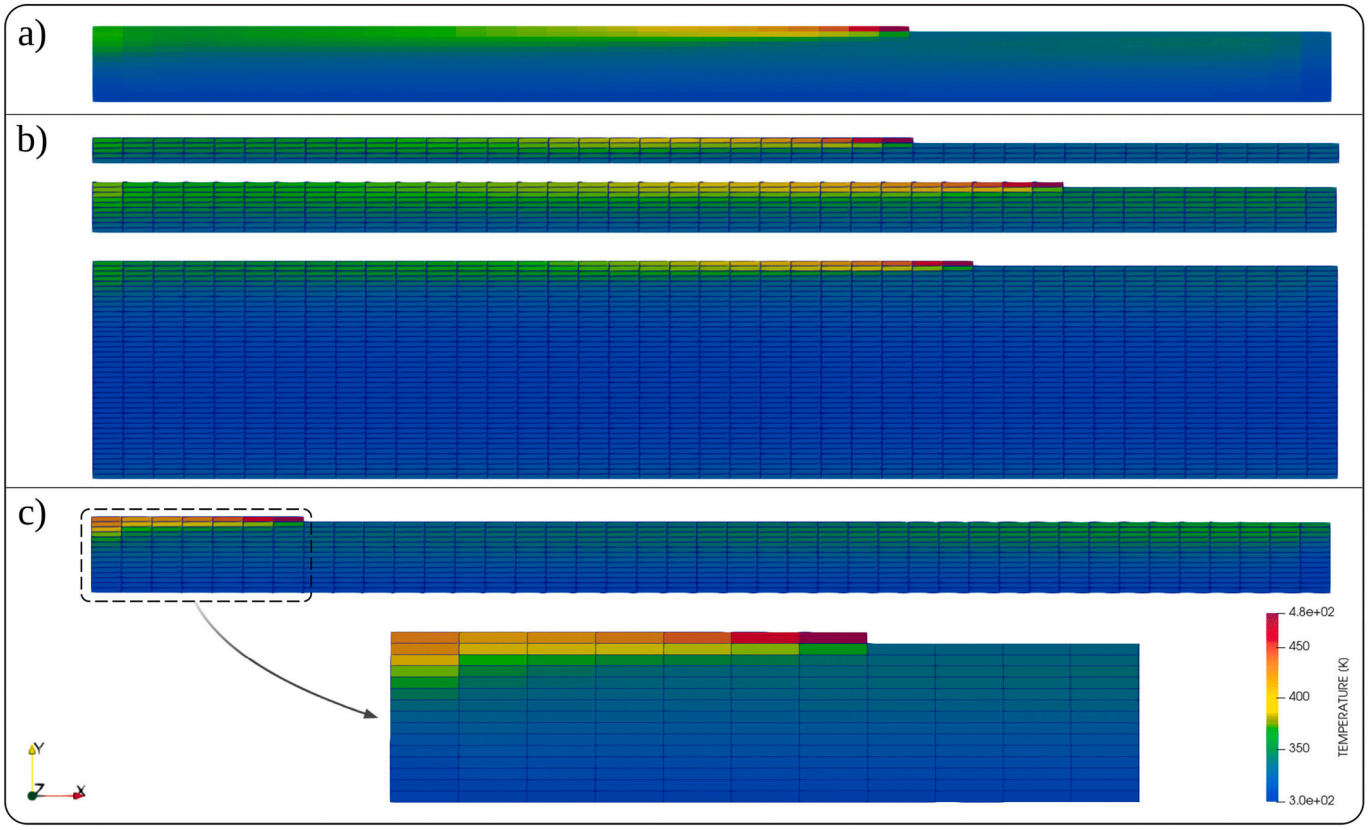

Fig. 5. Temperatures at some instances of the deposition process for the vertical wall: (a) general view, (b) layers 5, 10, and 43 as well as the presentation of CVs, (c) layer 15 with high resolution of CVs.

From these thermograms, the re-heating of previously deposited filaments depends on their location. As an example, deposition of the 43rd layer raises the temperature of approximately 4–5 layers, which is about 8–9 layers when the 10th layer is deposited; this is more obvious in Fig. 5(c) for the deposition of the 15th layer.

5.3. Experimental validation

In-process monitoring of temperature profile enables the local measurement of its distribution along with the consequence of deposition. This is carried out for a defined condition alongside with different locations of the proposed vertical wall.

In this set of experiments, the filament temperature profile is randomly recorded at some instants: Layer 5 (x = 30 mm, y = 1 mm), layer 20 (x = 20 mm, y = 4 mm), layer 37 (x = 35 mm, y = 7.4 mm), layer 54 (x = 40 mm, y = 10.8 mm), layer 63 (x = 25 mm, y = 12.6 mm), layer 88 (x = 40 mm, y = 17.6 mm). The liquefier temperature maintained at 210 °C as well as the platform temperature at 50 °C. Fig. 6 summarizes the obtained data by plotting the recorded temperature evolution as a function of time. In each case, as mentioned in the previous section, the cyclic temperature evolution of filaments varies based on their location. One key parameter to the cooling curve of all extracted data is that the influence of temperature radiation of the support/platform is observable, which is expected due to the nature of the means of measurement. Fig. 6 also plots the temperature distribution obtained by the prediction of the analytical model. Over a broad range of layers and various locations, there is a good agreement between the analytical model and the experimental data.

Regardless of cooling curves, the breath of temperature peaks is recorded and predicted by both approaches. However, the difference between the onset and relative magnitude of the peaks could be correlated to the nature of the measurement approach. Further, the peaks that themselves represent the existence of adhesion and contact of adjacent layers, become gradually smaller with time. On the other hand, as no phase changes were taken into account in the model, the released energy could be referred to as the difference of captured peaks.

Overall, based on the obtained prediction and recorded data, one can note that the cooling rate of previously deposited filament won't be affected after 4–5 deposition sequences; the higher the distance from platform, the higher the cooling rate predicted by the analytical approach. However, the recorded data represent a lower cooling rate in comparison with the obtained prediction. The main reasons could be listed as follows:

- The influence of the released energy due to phase change (both at melting and crystallization points) has an impact on the temperature profile of filaments.
- The platform plays an important role in the cooling stage of filaments (As of layer 5, in which there is a very good agreement between the two approaches).

5.4. Parametric studying

5.4.1. Influence of process parameters on temperature profile of filaments

- Liquefier temperature

The influence of liquefier temperature during layer deposition is considered first. A set of predictions is carried out where the filament is cooled at different liquefier temperatures. As it varies from $T_{Liq} = 200$ to 230 °C, greater values for the re-heating peaks are anticipated to shift the filament temperature profile around T_c. The predicted results indicate the same breadth, whereas, the variation of cooling rates is negligible. Clearly, as indicated in Fig. 7, the temperature profiles of the first

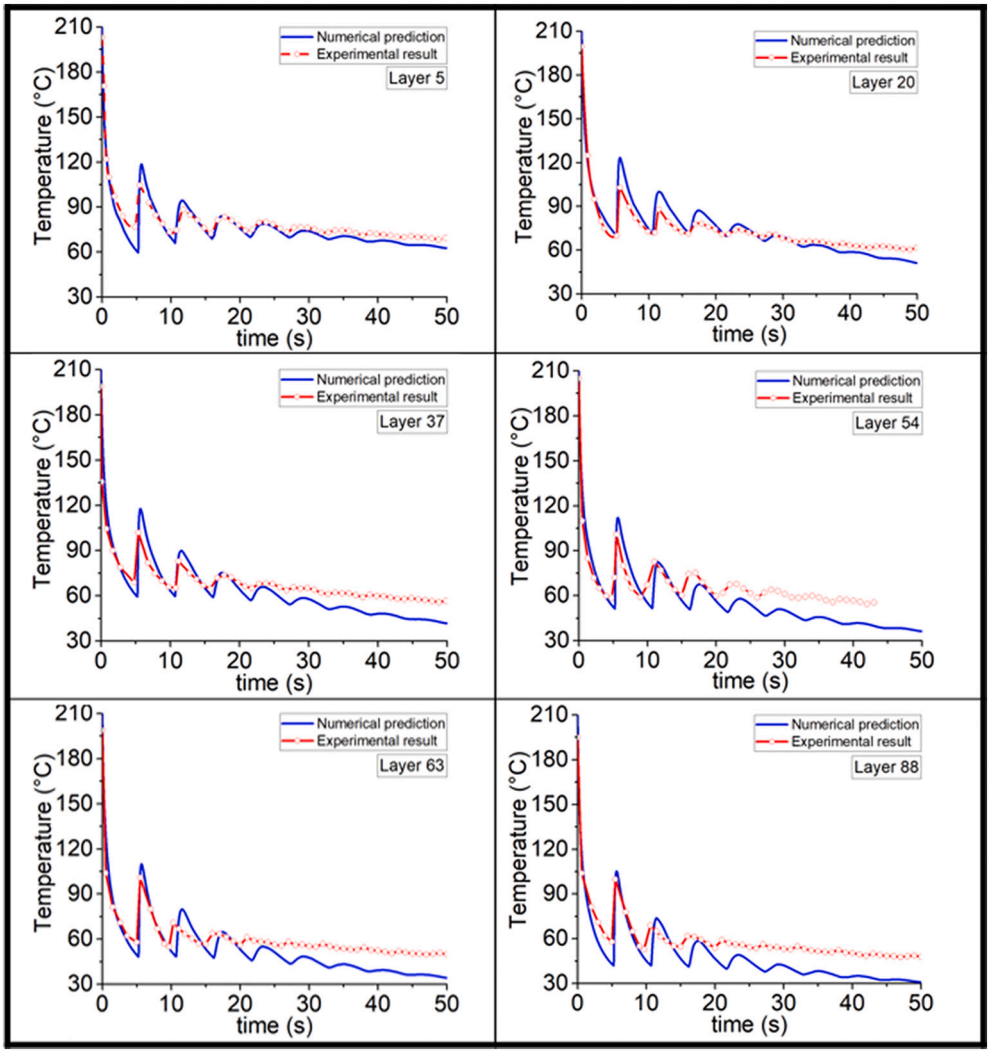

Fig. 6. Comparison of temperature evolution at different locations during the deposition of a vertical wall consisting of single filaments deposited on top of each other with prediction from theoretical model for various layer with specific locations.

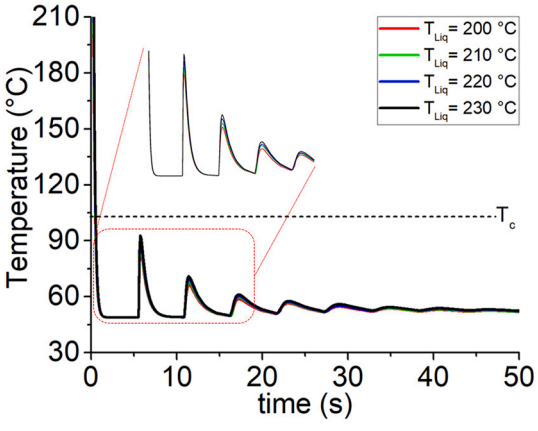

Fig. 7. The influence of liquefier temperature on temperature evolution during the deposition of a vertical wall consisting of single filaments deposited on top of each other with prediction obtained from theoretical model.

deposited layer (x = 30 mm) at different liquefier temperatures are so close to each other, which obviously represent the ineffectiveness of the relative variation of this parameter.

- Platform temperature

Furthermore, efforts are taken into account to consider the influence of platform temperature on temperature profile during deposition of the vertical wall (with the same condition as explained in the previous section). Fig. 8-a demonstrates the temperature profile by changing the platform temperature. As expected for the re-heating peaks, they all have identical onsets beside the great shift occurs by enhancing the platform temperature. Worth mentioning to say that the higher the platform temperature, the lower the cooling rate. Accordingly and unlike the observation that was taken into account by changing the liquefier temperature, the platform plays an important role in temperature evolution of filaments. In this case, the temperature profile is recorded experimentally at $T_{Platform}$ = 100 °C and compared with the results predicted by the analytical model (Fig. 8b). Presumably, the temperature varies around T_c, favorable adhesion of filaments. However, deformation and low quality of the printed part are important issues [49].

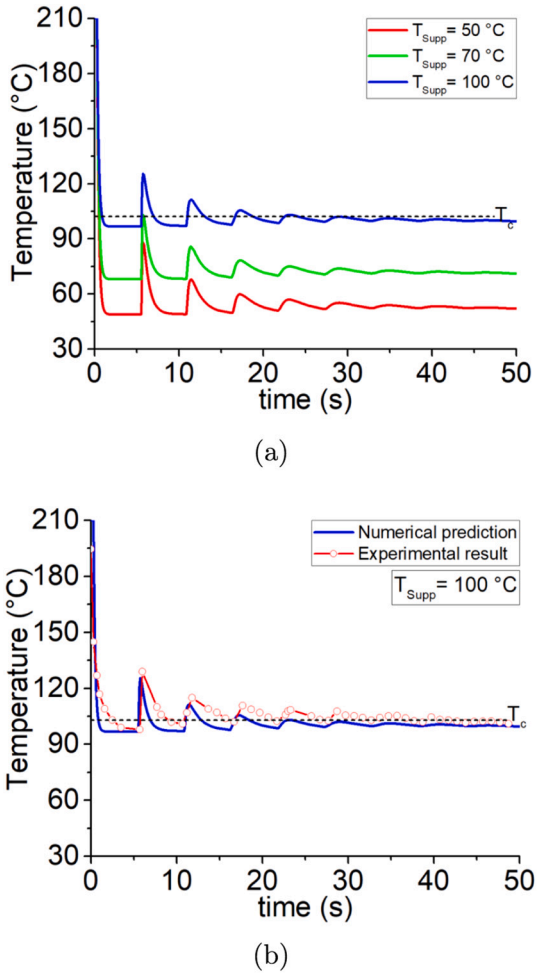

Fig. 8. The influence of platform temperature on temperature evolution during the deposition of a vertical wall consisting of single filaments deposited on top of each other with (a) prediction obtained from theoretical model and (b) experimental validation.

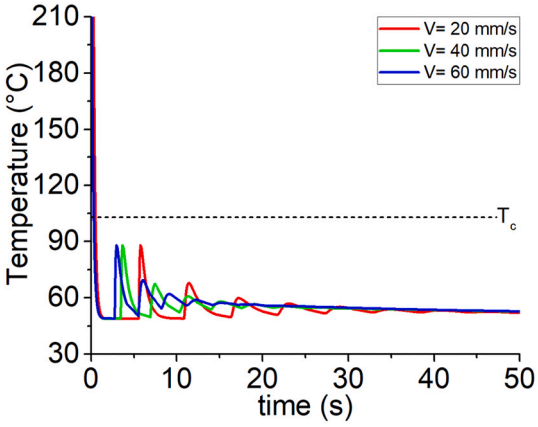

Fig. 9. The influence of print speed on temperature evolution during the deposition of a vertical wall consisting of single filaments deposited on top of each other with prediction obtained from theoretical model.

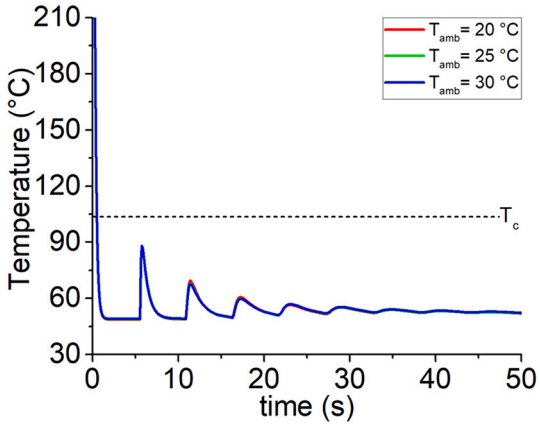

Fig. 10. The effect of ambient temperature on temperature evolution during the deposition of a vertical wall consisting of single filaments deposited on top of each other with prediction obtained from theoretical model.

- Print speed

The influence of print speed during filament deposition is evaluated next. Prediction is carried out where the filaments are printed in various speed of deposition V = 20, 40, and 60 mm/s. Similar to the predictions observed for variation of liquefier temperature, onsets of the peaks are approximately similar, whereas the cooling rate almost decreased by increasing the print speed (Fig. 9). The main characteristic of this parameter is that it helps raising the temperature profile of filaments and keeps them hot enough during the deposition sequences. Following previous studies [49,63], enhancing the print speed acts as a manner of a heating source by which it does not let the filament to be cooled down quickly. Also, worth mentioning to say that the onset of the peaks is found to arise at different times and thus their breadth is also decreased.

- Ambient temperature

Finally, predictions are carried out for investigating the influence of ambient temperature variation on heat transfer of filaments. Three values as T_{amb} = 20, 25, and 30 °C are utilized to compare and consider its effect. Fig. 10 presents the obtained results and similar to the liquefier temperature variation, there is not any change through the cooling rate and the re-heating peaks. This issue perhaps could be referred to as the in-capacitance of this parameter to have an impact on the temperature profile of filaments.

5.4.2. Optimization exploration with analytical model

The analytical heat transfer model introduced in Section 3, can be implemented for optimization purposes. The main advantage of the proposed model is that it is general and it could be implemented for various groups of materials, whether amorphous or semi-crystalline polymers, by considering complex geometry. Specifically, the role of various process parameters can be taken into account based on the experimentally validated model.

In the case of a semi-crystalline material (in our study: PLA), it is broadly believed that the defined time due to the cooling and re-heating of filaments is crucial for proper bonding to take place [64,65]. So, filaments must be hot enough, but not too hot, to avoid the deformation and reduced quality of the final part. Furthermore, the key assumption of the proposed analytical model is that the dynamic mesh is considered by the implementation of finite volume method. This issue corresponds

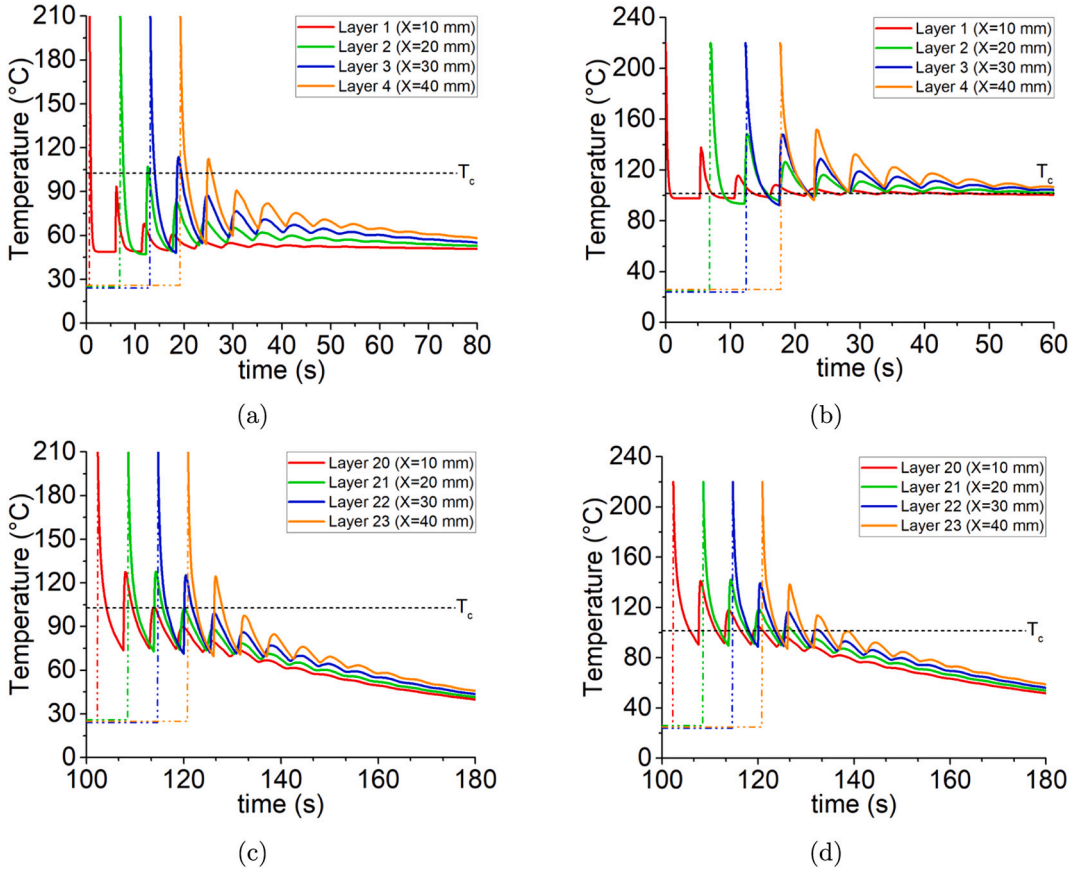

Fig. 11. Temperature evolution during the deposition of a vertical wall consisting of single filaments deposited on top of each other with prediction obtained from theoretical model for (a) layers 1–4, (b) optimized value for layers 1–4, (c) layers 20–23, and (d) optimized value for layers 20–23.

to the unsteady state heat transfer that exists in FFF.

To have a better understanding, extracted data from the prediction of analytical code is presented at real time of deposition (without synchronization of time at $t = 0$). Fig. 11(a, c) shows the temperature profile of layer 1–4, and layers 20–23. Parameter optimization using the values (T_{Liq} = 220 °C, $T_{Platform}$ = 70 °C, T_{amb} = 30 °C, V = 20 mm/s) is demonstrated in Fig. 11(b, d) for the same layers and locations. Fig. 10 (b) shows that temperature varies around T_c by implementing the mentioned values. This leads to the better crystallization of the printed layers and thus better adhesion, and favorable bonding. Unlikely, Fig. 11 (d) indicates that temperature varies for a period of time (about 20 s for each filament) around T_c and it drops again below T_c and hence cooling of material does not give sufficient time for crystallization and adhesion of layers. Seemingly, these differences can be resulted in the inhomogeneity of the printed structures and affect their strength through different layers.

Designed curves (Fig. 11(b, d)) demonstrate the capability of the analytical code presented here for accurate thermal analysis and further objectives. This could be used for optimization purposes by implementing all engaged parameters to have the possibility of improving the process to be resulted in bonding and adhesion enhancements. These results can also be used for consideration of temperature dependence viscosity and coalescence of filaments in rheological objectives.

With reference to the presented results in Fig. 11, the significance of heat transfer using the developed code toward the optimization of FFF process has been illustrated. The developed approach is a global code considering complex geometries, physical phenomena (e.g. solidification, re-melting, rheological behavior), and it is applicable to different types of polymeric/composite materials. Presenting the heat transfer using finite volume method (FVM), the temperature evolution of deposited filaments have been executed. Besides, the developed temperature measurement technique allows to implement the experimental data for validation purposes. The presented results is the first step of analytical prediction of filament bonding and strength of the 3D-printed parts. In our future work, we will focus on applying the obtained findings in adhesion (also known as coalescence) of filaments during deposition. The idea is to create a platform by considering the following issues:

- Heat transfer and cyclic temperature profile of deposited layers
- Physical phenomena such as phase transformation during cooling (and also re-heating) of deposited layers
- Temperature dependence viscosity of material during deposition
- Adhesion of deposited layers (coalescence of adjacent layers)

6. Conclusion

This paper investigates the heat transfer in (FFF)-3D printing process using both analytical modeling and experimental measurements. Heat transfer and temperature evolution of filaments play a key role in strength and adhesion of layers during deposition sequences. Results from this study can be applied for further objectives and help to identify the key process parameters that affect the heat transfer and thus the adhesion of layers. Predictions were validated experimentally using in-process monitoring of temperature profiles at the interface of filaments. The good agreement of the analytical model with the experimentally recorded data is encouraging. Results presented here help to develop the analytical predictions considering interaction of process parameters and also the rheological characteristics of the (FFF)-3D printing process.

Declaration of competing interest

The authors certify that they have no affiliations with or involvement in any organization or entity with any financial interest, or non-financial interest in the subject matter or materials discussed in this manuscript.

Acknowledgment

Figures were created with BioRender (biorender.com/).

Appendix A. Supplementary data

Supplementary data to this article can be found online at https://doi.org/10.1016/j.jmapro.2022.02.042.

References

[1] Dimitrov D, Schreve K, de Beer N. Advances in three dimensional printing–state of the art and future perspectives. Rapid Prototyp J 2006;12(3):136–47.
[2] Turner BN, Strong R, Gold SA. A review of melt extrusion additive manufacturing processes: I. Process design and modeling. Rapid Prototyp J 2014;20(3):192–204.
[3] El Magri A, El Mabrouk K, Vaudreuil S. Preparation and characterization of poly (ether ether ketone)/poly (ether imide)[peek/pei] blends for fused filament fabrication. J Mater Sci 2021;56:14348–67.
[4] Mohamed OA, Masood SH, Bhowmik JL. Optimization of fused deposition modeling process parameters for dimensional accuracy using i-optimality criterion. Measurement 2016;81:174–96.
[5] Khajavi SH, Holmström J, Partanen J. Additive manufacturing in the spare parts supply chain: hub configuration and technology maturity. Rapid Prototyp J 2018;24(7):1178–92.
[6] Macdonald E, Salas R, Espalin D, Perez M, Aguilera E, Muse D, Wicker RB. 3d printing for the rapid prototyping of structural electronics. IEEE Access 2014;2:234–42.
[7] Manapat JZ, Chen Q, Ye P, Advincula RC. 3d printing of polymer nanocomposites via stereolithography. Macromol Mater Eng 2017;302(9):1600553.
[8] Gao W, Zhang Y, Ramanujan D, Ramani K, Chen Y, Williams CB, Wang CC, Shin YC, Zhang S, Zavattieri PD. The status, challenges, and future of additive manufacturing in engineering. Comput Aided Des 2015;69:65–89.
[9] Iftikhar A, Khan M, Alam K, Imran Jaffery SH, Ali L, Ayaz Y, Khan A. Turbine blade manufacturing through rapid tooling (rt) process and its quality inspection. Mater Manuf Process 2013;28(5):534–8.
[10] El Magri A, Vanaei S, Shirinbayan M, Vaudreuil S, Tcharkhtchi A. An investigation to study the effect of process parameters on the strength and fatigue behavior of 3d-printed pla-graphene. Polymers 2021;13(19):3218.
[11] Nejad ZMousavi, Zamanian A, Saeidifar M, Vanaei HR, Amoli MSalar. 3d bioprinting of polycaprolactone-based scaffolds for pulp-dentin regeneration: investigation of physicochemical and biological behavior. Polymers 2021;13(24):4442.
[12] Yagnik D. Fused deposition modeling–a rapid prototyping technique for product cycle time reduction cost effectively in aerospace applications. IOSR J Mech Civ Eng 2014;5:62–8.
[13] Vanaei S, Parizi M, Salemizadehparizi F, Vanaei H. An overview on materials and techniques in 3d bioprinting toward biomedical application. Eng Regen 2021;2:1–18.
[14] El Magri A, Vanaei S, Vaudreuil S. An overview on the influence of process parameters through the characteristic of 3d-printed peek and pei parts. High Perform Polym 2021;33(8):862–80.
[15] Sohrabian M, Vaseghi M, Khaleghi H, Dehrooyeh S, Kohan MSA. Structural investigation of delicate-geometry fused deposition modeling additive manufacturing scaffolds: experiment and analytics. J Mater Eng Perform 2021;30:6529–41.
[16] Endo H, Umeno T. Study on the influence of temperature of extruder head on the strength of the fdm 3d printing model. J Rob Mechatronics 2017;29(4):767–71.
[17] Spoerk M, Arbeiter F, Cajner H, Sapkota J, Holzer C. Parametric optimization of intra-and inter-layer strengths in parts produced by extrusion-based additive manufacturing of poly (lactic acid). J Appl Polym Sci 2017;134(41):45401.
[18] Wang L, Gramlich WM, Gardner DJ. Improving the impact strength of poly (lactic acid)(pla) in fused layer modeling (flm). Polymer 2017;114:242–8.
[19] Song Y, Li Y, Song W, Yee K, Lee K-Y, Tagarielli VL. Measurements of the mechanical response of unidirectional 3d-printed pla. Mater Des 2017;123:154–64.
[20] Magri AE, El Mabrouk K, Vaudreuil S, Touhami ME. Mechanical properties of cf-reinforced pla parts manufactured by fused deposition modeling. J Thermoplast Compos Mater 2021;34(5):581–95.
[21] Magri AEl, Mabrouk KEl, Vaudreuil S, Touhami MEbn. Experimental investigation and optimization of printing parameters of 3d printed polyphenylene sulfide through response surface methodology. J Appl Polym Sci 2021;138(1):49625.
[22] Altan M, Eryildiz M, Gumus B, Kahraman Y. Effects of process parameters on the quality of pla products fabricated by fused deposition modeling (fdm): surface roughness and tensile strength. Mater Test 2018;60(5):471–7.
[23] Chacón J, Caminero MA, Garca-Plaza E, Núñez PJ. Additive manufacturing of pla structures using fused deposition modelling: effect of process parameters on mechanical properties and their optimal selection. Mater Des 2017;124:143–57.
[24] Gomez-Gras G, Jerez-Mesa R, Travieso-Rodriguez JA, Lluma-Fuentes J. Fatigue performance of fused filament fabrication pla specimens. Mater Des 2018;140:278–85.
[25] Tsouknidas A, Pantazopoulos M, Katsoulis I, Fasnakis D, Maropoulos S, Michailidis N. Impact absorption capacity of 3d-printed components fabricated by fused deposition modelling. Mater Des 2016;102:41–4.
[26] Wu W, Geng P, Li G, Zhao D, Zhang H, Zhao J. Influence of layer thickness and raster angle on the mechanical properties of 3d-printed peek and a comparative mechanical study between peek and abs. Materials 2015;8(9):5834–46.
[27] Magri AEl, Vaudreuil S, Mabrouk KEl, Touhami ME. Printing temperature effects on the structural and mechanical performances of 3d printed poly-(phenylene sulfide) material. In: IOP Conference Series: Materials Science and Engineering. vol. 783. IOP Publishing; 2020. p. 1–6.
[28] Tran N-H, Nguyen V-N, Ngo A-V, Nguyen V-C. Study on the effect of fused deposition modeling (fdm) process parameters on the printed part quality. Int J Eng Res Appl 2017;7(12):71–7.
[29] Peng F, Vogt BD, Cakmak M. Complex flow and temperature history during melt extrusion in material extrusion additive manufacturing. Addit Manuf 2018;22:197–206.
[30] Prajapati H, Ravoori D, Woods RL, Jain A. Measurement of anisotropic thermal conductivity and inter-layer thermal contact resistance in polymer fused deposition modeling (fdm). Addit Manuf 2018;21:84–90.
[31] Yardimci MA, Güçeri S. Conceptual framework for the thermal process modelling of fused deposition. Rapid Prototyp J 1996;2(2):26–31.
[32] Ravoori D, Alba L, Prajapati H, Jain A. Investigation of process-structure-property relationships in polymer extrusion based additive manufacturing through in situ high speed imaging and thermal conductivity measurements. Addit Manuf 2018;23:132–9.
[33] Naghieh S, Ravari MK, Badrossamay M, Foroozmehr E, Kadkhodaei M. Numerical investigation of the mechanical properties of the additive manufactured bone scaffolds fabricated by fdm: the effect of layer penetration and post-heating. J Mech Behav Biomed Mater 2016;59:241–50.
[34] Pandey PM, Venkata Reddy N, Dhande SG. Virtual hybrid-fdm system to enhance surface finish. Virtual Phys Prototyp 2006;1(2):101–16.
[35] Pal D, Ravi B. Rapid tooling route selection and evaluation for sand and investment casting. Virtual Phys Prototyp 2007;2(4):197–207.
[36] Widden M, Gunn K. Design–build–test of model aerofoils for engineering education using fdm. Virtual Phys Prototyp 2010;5(4):189–94.
[37] El Magri A, El Mabrouk K, Vaudreuil S, Chibane H, Touhami ME. Optimization of printing parameters for improvement of mechanical and thermal performances of 3d printed poly (ether ether ketone) parts. J Appl Polym Sci 2020;137(37):49087.
[38] Bellehumeur C, Li L, Sun Q, Gu P. Modeling of bond formation between polymer filaments in the fused deposition modeling process. J Manuf Process 2004;6(2):170–8.
[39] Bellehumeur C, Bisaria M, Vlachopoulos J. An experimental study and model assessment of polymer sintering. Polym Eng Sci 1996;36(17):2198–207.
[40] Sun Q, Rizvi G, Bellehumeur C, Gu P. Effect of processing conditions on the bonding quality of fdm polymer filaments. Rapid Prototyp J 2008;14(2):72–80.
[41] Zaldivar R, Witkin D, McLouth T, Patel D, Schmitt K, Nokes J. Influence of processing and orientation print effects on the mechanical and thermal behavior of 3d-printed ultem 9085 material. Addit Manuf 2017;13:71–80.
[42] D'Amico A, Peterson AM. An adaptable fea simulation of material extrusion additive manufacturing heat transfer in 3d. Addit Manuf 2018;21:422–30.
[43] Costa S, Duarte F, Covas J. Estimation of filament temperature and adhesion development in fused deposition techniques. J Mater Process Technol 2017;245:167–79.
[44] Vanaei HR, Shirinbayan M, Deligant M, Khelladi S, Tcharkhtchi A. In-process monitoring of temperature evolution during fused filament fabrication: a journey from numerical to experimental approaches. Thermo 2021;1(3):332–60.
[45] Mackay ME, Swain ZR, Banbury CR, Phan DD, Edwards DA. The performance of the hot end in a plasticating 3d printer. J Rheol 2017;61(2):229–36.
[46] Bellini A, Güçeri S. Mechanical characterization of parts fabricated using fused deposition modeling. Rapid Prototyp J 2003;9(4):252–64.
[47] Rodrguez JF, Thomas JP, Renaud JE. Design of fused-deposition abs components for stiffness and strength. J Mech Des 2003;125(3):545–51.
[48] Kousiatza C, Karalekas D. In-situ monitoring of strain and temperature distributions during fused deposition modeling process. Mater Des 2016;97:400–6.
[49] Vanaei H, Shirinbayan M, Deligant M, Raissi K, Fitoussi J, Khelladi S, Tcharkhtchi A. Influence of process parameters on thermal and mechanical properties of polylactic acid fabricated by fused filament fabrication. Polym Eng Sci 2020;60(8):1822–31.
[50] Malekipour E, Attoye S, El-Mounayri H. Investigation of layer based thermal behavior in fused deposition modeling process by infrared thermography. Procedia Manuf 2018;26:1014–22.
[51] Wolszczak P, Lygas K, Paszko M, Wach RA. Heat distribution in material during fused deposition modelling. Rapid Prototyp J 2018;24(3):615–22.
[52] Vanaei H, Deligant M, Shirinbayan M, Raissi K, Fitoussi J, Khelladi S, Tcharkhtchi A. A comparative in-process monitoring of temperature profile in fused filament fabrication. Polym Eng Sci 2021;61(1):68–76.
[53] Ferraris E, Zhang J, Van Hooreweder B. Thermography based in-process monitoring of fused filament fabrication of polymeric parts. CIRP Ann 2019;68(1):213–6.

[54] Vanaei HR, Shirinbayan M, Costa SF, Duarte FM, Covas JA, Deligant M, Khelladi S, Tcharkhtchi A. Experimental study of pla thermal behavior during fused filament fabrication. J Appl Polym Sci 2021;138(4):49747.
[55] Pantankar S, Spalding D. A calculation procedure for heat, mass and momentum transfer in three-dimensional parabolic flows. Int J Heat Mass Transf 1972;15: 54–73.
[56] Deligant M, Specklin M, Khelladi S. A naturally anti-diffusive compressible two phases kapila model with boundedness preservation coupled to a high order finite volume solver. Comput Fluids 2015;114:265–73.
[57] Deligant M, Nogueira Garea X, Khelladi S, Sauret E, Reding B. Toward a high resolution real gas finite volume solver with multi optimal order detection. In: Proceedings of the 5th International Seminar on ORC Power Systems. The National Technical University of Athens (NTUA); 2019. p. 1–9.
[58] Ramirez L, Nogueira X, Khelladi S, Chassaing J-C, Colominas I. A new higher-order finite volume method based on moving least squares for the resolution of the incompressible navier–stokes equations on unstructured grids. Comput Methods Appl Mech Eng 2014;278:883–901.
[59] Vanaei HR, Shirinbayan M, Vanaei S, Fitoussi J, Khelladi S, Tcharkhtchi A. Multi-scale damage analysis and fatigue behavior of pla manufactured by fused deposition modeling (fdm). Rapid Prototyp J 2021;27(2):371–8.
[60] Costa S, Duarte F, Covas J. Towards modelling of free form extrusion: analytical solution of transient heat transfer. Int J Mater Form 2008;1(1):703–6.
[61] Rodrguez JF, Thomas JP, Renaud JE. Mechanical behavior of acrylonitrile butadiene styrene (abs) fused deposition materials. Experimental investigation. Rapid Prototyp J 2001;7(3):148–58.
[62] Kraus AD, Aziz A, Welty J, Sekulic D. Extended surface heat transfer. Appl Mech Rev 2001;54(5):B92.
[63] Vanaei H, Raissi K, Deligant M, Shirinbayan M, Fitoussi J, Khelladi S, Tcharkhtchi A. Toward the understanding of temperature effect on bonding strength, dimensions and geometry of 3d-printed parts. J Mater Sci 2020;55(29): 14677–89.
[64] Hopper RW. Coalescence of two equal cylinders: exact results for creeping viscous plane flow driven by capillarity. J Am Ceram Soc 1984;67(12). C–262.
[65] Rosenzweig N, Narkis M. Sintering rheology of amorphous polymers. Polym Eng Sci 1981;21(17):1167–70.